Bang-Bang Control Of Spherical Variable-Shape Buoy Wave Energy Converters*

Mohamed A. Shabara[1] and Ossama Abdelkhalik[2]

***Abstract*— The study of variable-shape wave energy converters has been receiving more attention recently. In this work, a dynamic model for axisymmetric Variable-Shape Buoy Wave Energy Converters is derived within the context of Lagrangian mechanics. The assumed modes method is used to approximate the flexible modes of the buoy. The bang-bang control algorithm is implemented to power take-off unit. A numerical simulation case study is presented that demonstrates the utility of the developed model in studying the behavior of the flexible shell buoy and the overall performance of the spherical Variable-Shape buoy Wave Energy Converter.**

I. INTRODUCTION

The increase in future energy demand will result in an increase in energy production from renewable and non-renewable sources [1]. The U.S. Energy Information Administration reported that electricity generation by fossil fuels was 60.3% in 2020. And to increase the renewable energy share, more efficient energy harvesting, and storage technologies have to be produced to in the future energy production distribution percentages.

Since 1799, multiple Wave Energy Converters (WECs) are introduced in [2]. These WECs are classified based on their theory of operation, their closeness to shore, or flexibility/rigidity of shells. One of the most used devices is the point absorbs (PA). Heave only point observers [3] structure are made of floating buoy connected to a power take-off unit. The power take-off unit (PTO) can be a hydraulic cylinder either attached to a frame on the seabed in shallow waters or attached to a suspended structure few meters below the sea level with little movement. The hydraulic fluid is pumped by the PTO that drives a hydraulic motor coupled with an electric generator.

The most common approach to simulate the Fluid-Structure Interaction (FSI) is by coupling computational fluid dynamics (CFD) solvers with finite element analysis solvers (FEA); this is usually done using commercial software like ANSYS [4]. Another approach is to couple a boundary value problem (BVP) solver with a structural model that can predict elastic finite element response [5]. However, these aforementioned methods are computationally expensive. On the other hand, the generalized modes methods are computationally less expensive where a reduced-order structural dynamics WEC system is included in the BVP solver. In this method, the additional degrees of freedom (DOF) associated with a pre-selected set of generalized body modes are included in the frequency domain hydrodynamic solver [6], [7].

Reference [4] presents high fidelity simulations using two-way fluid-structure interaction by coupling a CFD solver (FLUENT) with the Mechanical ANSYS APDL. A passive control system was applied to the control force, and the performance of the spherical Variable shape wave energy converters (VSB WEC) was evaluated and compared to a corresponding Fixed-Shape Wave energy converter (FSB WEC). The results showed that the energy harvesting by the VSB WEC significantly increased by 7.96% over 30 sec compared to the FSB WEC.

The rate of change of the difference in the harvested energies of the VSB and FSB WECs in [4] increased during the first 20 sec of the simulations compared to the last 10 seconds, suggesting more impact for the transient periods. These results encourage the utilization of latch control or bang-bang control algorithms [8], [9] to the VSB WEC to excite the shell's natural frequencies.

Reference [9] introduced an optimal control approach for FSB WECs point absorbs. A hybrid control system that combines the bang-bang control and singular arc control was found to harvest more power than using any of them individually.

In this article, a simplified dynamic model for spherical VSB WECs is developed using Lagrangian mechanics. The approximated modes method along with Legendre Polynomials are utilized to derive the equations of motion for VSB WECs. This model assumes no rotation and focuses on the heave-only movement. This model also ignores the holonomic constraints and other external forces acting on the WEC shell, other than the buoyant and excitation forces. The VSB WEC performance is then evaluated with Bang-Bang control on the Power Take-Off unit (PTO) in simple regular waves.

II. NOTATIONS

A set of reference frames shall be introduced to describe an infinitesimal mass on the VSB WECs' shell with respect to an inertial reference frame. An inertial reference frame $\hat{\boldsymbol{a}}$ is fixed at a reference position away from the VSB WEC, as shown in Fig. (1). This reference frame can be either placed on the seabed or at any non-moving reference position. The inertial reference frame is represented as:

*This work was supported by National Science Foundation (NSF).

[1]Mohamed A. Shabara is a PhD student in the department of Aerospace Engineering, Iowa State University, Iowa, IA 50011, USA mshabara@iastate.edu

[2]Ossama Abdelkhalik. Associate professor with the Department of Aerospace Engineering, Iowa State University, Iowa, IA 50011, USA ossama@iastate.edu

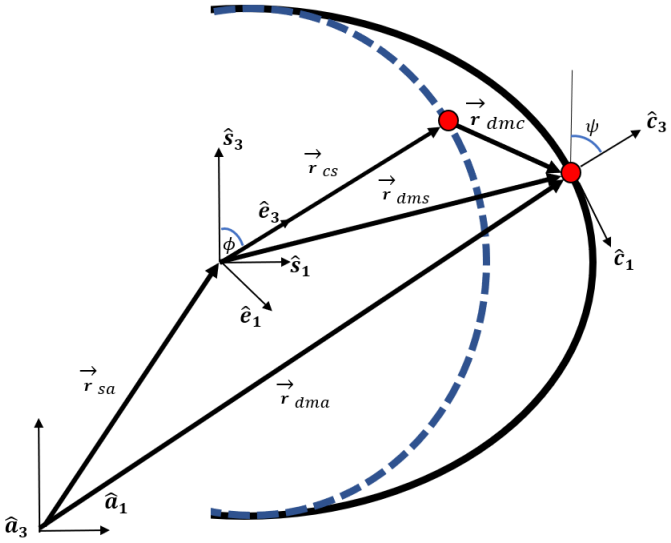

Fig. 1: Deformed (Black) and Undeformed Shells (Blue)

$$\hat{\boldsymbol{a}} = \begin{bmatrix} \hat{\boldsymbol{a}}_1 & \hat{\boldsymbol{a}}_2 & \hat{\boldsymbol{a}}_3 \end{bmatrix}$$

In addition, a body reference frame $\hat{\boldsymbol{s}}$ attached to the buoy's center of mass is defined, as shown in Fig. (1). Furthermore, a reference frame "$\hat{\boldsymbol{e}}$" is attached to the origin of the $\hat{\boldsymbol{s}}$ frame such that $\hat{\boldsymbol{e}}_3$ always points at an infinitesimal mass on the undeformed buoy . Noting that, the angle between the reference frames axes $\hat{\boldsymbol{s}}_3$ and $\hat{\boldsymbol{e}}_3$ is ϕ. This angle ϕ does not change in real-time.

The reference frame $\hat{\boldsymbol{c}}$ is attached to a deformed infinitesimal mass with $\hat{\boldsymbol{c}}_3$ perpendicular to the deformed buoy. The angle ψ is the angle between $\hat{\boldsymbol{s}}_3$ and $\hat{\boldsymbol{c}}_3$. Due to the axisymmetric assumption for the WEC deformation, all the second components of the aforementioned reference frames are always pointing inside the page, as demonstrated in Fig. (1).

III. VSB WEC Kinematics

The deformation vector of an infinitesimal mass can be described by $\vec{\boldsymbol{r}}_{dmc}(\phi, t)$ such that:

$$\vec{\boldsymbol{r}}_{dmc}(\phi, t) = \begin{bmatrix} u_\phi(\phi, t) & 0 & u_r(\phi, t) \end{bmatrix}^T \tag{1}$$

where $u_\phi(\phi, t)$ and $u_r(\phi, t)$ are the displacement in the $\hat{\boldsymbol{e}}_1$ and $\hat{\boldsymbol{e}}_3$ directions, respectively (Fig. 1). These vectors are computed using the approximated modes method as:

$$\begin{aligned} u_\phi(\phi, t) &= \sum_{n=1}^{N} \Psi_n^\phi(\phi)\eta_n(t) \\ &= \underbrace{\begin{bmatrix} \Psi_1^\phi \dots \Psi_N^\phi \end{bmatrix}}_{\boldsymbol{\Psi}^\phi} \underbrace{\begin{bmatrix} \eta_1(t) \\ \vdots \\ \eta_N(t) \end{bmatrix}}_{\boldsymbol{\eta}(t)} = \boldsymbol{\Psi}^\phi(\phi)\boldsymbol{\eta}(t) \end{aligned} \tag{2}$$

$$\begin{aligned} u_r(\phi, t) &= \sum_{n=1}^{N} \Psi_n^r(\phi)\eta_n(t) \\ &= \underbrace{\begin{bmatrix} \Psi_1^r \dots \Psi_N^r \end{bmatrix}}_{\boldsymbol{\Psi}^r} \underbrace{\begin{bmatrix} \eta_1(t) \\ \vdots \\ \eta_N(t) \end{bmatrix}}_{\boldsymbol{\eta}(t)} = \boldsymbol{\Psi}^r(\phi)\boldsymbol{\eta}(t) \end{aligned} \tag{3}$$

where N is the number of prescribed polynomials. $\boldsymbol{\eta}(t)$ is unknown functions of time, and $\boldsymbol{\Psi}^\phi(\phi)$ and $\boldsymbol{\Psi}^r(\phi)$ are trial functions.

Combining Eq. (1) with Eqs. (2) and (5), we get:

$$\vec{\boldsymbol{r}}_{dmc}(\phi, t) = \begin{bmatrix} \boldsymbol{\Psi}^\phi \\ \boldsymbol{0} \\ \boldsymbol{\Psi}^r \end{bmatrix} \boldsymbol{\eta} = \boldsymbol{\Phi}_e \boldsymbol{\eta} \tag{4}$$

Eqs. (5) and (6) represent the shape (trial) functions composed of Legendre polynomials of the first type as they satisfy the geometric boundary conditions of the VSB [10], [11].

$$\Psi_n^\phi(\phi) = \frac{dP_n(\cos(\phi))}{d\phi} \tag{5}$$

$$\Psi_n^r(\phi) = \frac{(1 + (1 + \nu))\Omega_n^2}{1 - \Omega_n^2} P_n(\cos(\phi)) \tag{6}$$

where for thin shells Ω_n is expressed as [10]:

$$\begin{aligned} {\Omega_n}^2{}_{1,2} = &\frac{1}{2(1-\nu)} n(n+1) + 1 + 3\nu \\ &\pm \sqrt{[n(n+1) + 1 + 3\nu]^2 - 4(1-\nu^2)[n(n+1) - 2]} \end{aligned} \tag{7}$$

where ν is Poisson's ratio. From Fig. (1), the vector describing the location of an infinitesimal mass on the deformed shell in the inertial frame is expressed as:

$$\vec{\boldsymbol{r}}_{dma} = \vec{\boldsymbol{r}}_{sa} + \vec{\boldsymbol{r}}_{cs} + \vec{\boldsymbol{r}}_{dmc} \tag{8}$$

and its derivative after applying the transport theorem is:

$${}^a\dot{\vec{\boldsymbol{r}}}_{dma} = C_{sa}\, {}^a\dot{\vec{\boldsymbol{r}}}_{sa} + C_{se}\boldsymbol{\Phi}_e\dot{\boldsymbol{\eta}} - [C_{se}({}^e\vec{\boldsymbol{r}}_{cs} + {}^e\vec{\boldsymbol{r}}_{dmc})]^\times \vec{\omega}_{as} \tag{9}$$

where C_{ij} is a transformation from the j^{th} to the i^{th} reference frame. Assuming that the buoy does not undergo any rotations, Eq. (10) can be reduced to

$${}^a\dot{\vec{\boldsymbol{r}}}_{dma} = C_{sa}\, {}^a\dot{\vec{\boldsymbol{r}}}_{sa} + C_{se}\boldsymbol{\Phi}_e\dot{\boldsymbol{\eta}} \tag{10}$$

IV. The Equation of Motion of VSB WEC

The equations of motion for VSB WEC point absorber is derived in this section (heave only) using lagrangian mechanics. This is done by calculating the total kinetic, the total potential, and the total strain energies; subsequently, applying Lagrange Equation expressed in Eq. (11) yields the desired equation of motion:

$$\frac{d}{dt}\left(\frac{\partial \mathcal{L}}{\partial \dot{\vec{\mathbf{x}}}}\right) - \frac{\partial \mathcal{L}}{\partial \vec{\mathbf{x}}} = \boldsymbol{Q} \tag{11}$$

where $\boldsymbol{Q}$ is the generalized external force.

A. Total Kinetic Energy Calculation

The kinetic energies in the system arise from two main motions; the translation motion of the CG and the deformation of the buoy's shell. The total kinetic energy is calculated using the following integral:

$$\mathcal{T} = \frac{1}{2}\int_S {}^a\dot{\vec{\boldsymbol{r}}}_{dma} \cdot {}^a\dot{\vec{\boldsymbol{r}}}_{dma} dm \tag{12}$$

After carrying out the dot product and integration with respect to the buoy's mass, then ignoring all the terms associated with the product of ${}^a\dot{\vec{\boldsymbol{r}}}_{sa}$ and $\dot{\boldsymbol{\eta}}$, we get:

$$\mathcal{T} = \frac{1}{2}\dot{\vec{\mathbf{x}}}^T \underbrace{\begin{bmatrix} \mathbf{1}\, m & \mathbf{0} \\ \mathbf{0} & \boldsymbol{M}_e \end{bmatrix}}_{\boldsymbol{M}} \dot{\vec{\mathbf{x}}} \tag{13}$$

$$= \frac{1}{2}\dot{\mathbf{x}}^T \boldsymbol{M} \dot{\vec{\mathbf{x}}} \tag{14}$$

where $\boldsymbol{M}$ is the total system mass matrix, m is the VSB WEC mass, and $\mathbf{1} = \begin{bmatrix}\mathbf{1}_1 & \mathbf{1}_2 & \mathbf{1}_3\end{bmatrix}$ is an identity matrix. Also, the vector of generalized coordinates $\dot{\vec{\mathbf{x}}}$ and $\boldsymbol{M_e}$ are expressed as [11]–[13]:

$$\dot{\vec{\mathbf{x}}} = \begin{bmatrix} {}^a\dot{\vec{\boldsymbol{r}}}_{sa} & \dot{\boldsymbol{\eta}} \end{bmatrix}^T \tag{15}$$

$$\boldsymbol{M}_e = 2\pi\rho h \int_0^\pi \left\{ \left(\boldsymbol{\Psi}^{\phi^T} \boldsymbol{\Psi}^{\phi} + \boldsymbol{\Psi}^{r^T} \boldsymbol{\Psi}^{r} \right) r^2 \sin\phi \right\} d\phi \tag{16}$$

where r and h are the buoy's shell external radius and thickness, respectively, and ρ is the material density.

B. Total Potential Energy Calculation

The total potential energy of the buoy is the combination of two energies, the gravitational energy, and the strain energy, as shown in Eq. (17).

$$\mathcal{V} = \frac{1}{2}\boldsymbol{\eta}^T \boldsymbol{K}_e \boldsymbol{\eta} + mg\mathbf{1}_3^T \vec{\boldsymbol{r}}_{sa} \tag{17}$$

where $\boldsymbol{K}_e$ is the stiffness matrix of the buoy's shell, and it is calculated using the following equation [11], [13]:

$$\boldsymbol{K}_e = \frac{2\pi E h}{1-\nu^2}\int_0^\pi \{\zeta^{\phi\phi^T}\zeta^{\phi\phi} + \zeta^{\theta\theta^T}\zeta^{\theta\theta} + \nu\left(\zeta^{\phi\phi^T}\zeta^{\phi\phi} + \zeta^{\theta\theta^T}\zeta^{\theta\theta}\right) r^2 \sin\phi\} d\phi \tag{18}$$

where

$$\zeta^{\phi\phi} = \frac{1}{r}\left(\frac{\partial \Psi^\phi}{\partial \phi} + \Psi^r\right)$$

$$\zeta^{\theta\theta} = \frac{1}{r}\left(\Psi^\phi \cot(\phi) + \Psi^r\right)$$

By subtracting Eqs. (14) and (17), the Lagrangian for the full system can be expressed as [13], [14]:

$$\mathcal{L} = \mathcal{T} - \mathcal{V} = \frac{1}{2}\dot{\vec{\mathbf{x}}}^T \boldsymbol{M} \dot{\vec{\mathbf{x}}} - \vec{\mathbf{x}}^T \begin{bmatrix} mg\mathbf{1}_3 \\ \frac{1}{2}\boldsymbol{\eta}^T \boldsymbol{K}_e \end{bmatrix} \tag{19}$$

From Eqs. (19) and (11) we can write:

$$\frac{\partial \mathcal{L}}{\partial \vec{\mathbf{x}}} = -\begin{bmatrix} mg\mathbf{1}_3 & \boldsymbol{K}_e\boldsymbol{\eta} \end{bmatrix}^T \tag{20}$$

$$\frac{d}{dt}\left(\frac{\partial \mathcal{L}}{\partial \dot{\vec{\mathbf{x}}}}\right) = \frac{d}{dt}\left(\boldsymbol{M}\dot{\vec{\mathbf{x}}}\right) = \boldsymbol{M}\ddot{\vec{\mathbf{x}}} \tag{21}$$

And therefore:

$$\boldsymbol{M}\ddot{\vec{\mathbf{x}}} + \boldsymbol{D}\dot{\vec{\mathbf{x}}} + \mathbf{a} = \boldsymbol{Q} \tag{22}$$

$$= \boldsymbol{Q}_{pto} + \boldsymbol{Q}_{hydro} \tag{23}$$

where

$$\vec{\mathbf{x}} = \begin{bmatrix} \vec{\boldsymbol{r}}_{sa} & \boldsymbol{\eta} \end{bmatrix}^T \tag{24}$$

$$\boldsymbol{a} = \begin{bmatrix} mg\mathbf{1}_3 & \boldsymbol{K}_e\boldsymbol{\eta} \end{bmatrix}^T \tag{25}$$

$$\boldsymbol{D} = \text{diag}\{\boldsymbol{D}_x \quad \boldsymbol{D}_e\}_{(3+N)\times(3+N)} \tag{26}$$

$\vec{\mathbf{x}}$ is the vector of generalized coordinates, $\boldsymbol{D}$ is the damping matrix that accounts for the transnational $\boldsymbol{D}_x$ and internal material damping $\boldsymbol{D}_e$ matrices. $\boldsymbol{Q}_{pto}$ is the generalized control force and $\boldsymbol{Q}_{hydro}$ is the generalized hydrodynamic force.

In the following subsections, regular excitation waves and bang-bang PTO force will be applied on the WEC.

C. Power Take-off Unit Force

The bang-bang control can take the form [9]

$$\vec{\boldsymbol{f}}^{pto} = \begin{cases} -\gamma, & {}^a\dot{\vec{r}}_{sa3} > 0 \\ \gamma, & {}^a\dot{\vec{r}}_{sa3} < 0 \end{cases} \tag{27}$$

where γ is the maximum thrust used in the bang-bang control. The virtual work of the VSB WEC is calculated as the multiplication of force and distance as follows [13], [14]:

$$\delta W_{pto} = \sum_{j=1}^{n} Q_j^{pto} \delta x_j \tag{28}$$

where

$$Q_j^{pto} = \vec{\boldsymbol{f}}^{pto} \cdot \frac{\partial \vec{\boldsymbol{r}}_{sa}}{\partial q_j},\ \forall j = 1, \cdots 3+N \tag{29}$$

and in the matrix form, can be expressed as:

$$\begin{aligned}\delta W_{pto} &= \vec{\boldsymbol{f}}^{pto} \cdot \delta \vec{\boldsymbol{r}}_{sa} = \delta \vec{\boldsymbol{r}}_{sa}^{T} \vec{\boldsymbol{f}}^{pto} \\ &= \begin{bmatrix} \delta \vec{\boldsymbol{r}}_{sa}^{T} & \delta \boldsymbol{\eta}^{T} \end{bmatrix} \begin{bmatrix} \vec{\boldsymbol{f}}^{pto} \\ \mathbf{0}_{N\times 1} \end{bmatrix} \\ &= \begin{bmatrix} \delta \vec{\boldsymbol{r}}_{sa}^{T} & \delta \boldsymbol{\eta} \end{bmatrix} \begin{bmatrix} sign(^{a}\dot{\vec{r}}_{sa3})\, \gamma\, \mathbf{1}_3 \\ \mathbf{0}_{N\times 1} \end{bmatrix} \\ &= \delta \vec{\mathbf{x}}^{T} \boldsymbol{Q}_{pto}\end{aligned}$$

D. Hydrodynamic Forces

Only two forces are assumed to act on the flexible buoy shell: the buoyant and the regular excitation forces. The submerged volume of the VSB changes continuously with time; to calculate this submerged volume, the buoy is divided into a set of horizontal disks (partitions).

The buoyant force acting on the i^{th} partition is calculated using Eq. (30)

$$F_{bi} = \rho_w V_{si} g \tag{30}$$

Afterward, the trapezoidal rule is used to calculate the total submerged volume. The volume of the i^{th} disk is calculated as:

$$V_{si} = \pi \left(\frac{r_{dms1i} + r_{dms1i-1}}{2} \right)^2 \times r_{dms3i} \tag{31}$$

The excitation force on the i^{th} disk is calculated by Eq. (32),

$$F_{exi} = f_{exi} \cos \omega t = P_{ex} A_i \cos \omega t \tag{32}$$

where P_{ex} is the excitation pressure; uniform excitation pressure distribution around the buoy is assumed, and A_i is the circumferential surface area of the i^{th} disk and is calculated by the trapezoidal rule using Eq. (33)

$$A_i = 2\pi \left(\frac{\|\vec{\boldsymbol{r}}_{dms}\|_i + \|\vec{\boldsymbol{r}}_{dms}\|_{i-1}}{2} \right) \times r_{dms3i} \tag{33}$$

The trapezoidal rule used in the volumes and areas calculations is a second-order accurate method; to increase the accuracy of the calculation, a refinement loop is performed such that the size of the partitions is refined until there is a negligible change in the calculated total submerged volume/area at every time step.

The hydrodynamic force $\vec{\boldsymbol{f}}_{hydro}$ is expressed as

$$\vec{\boldsymbol{f}}_{hydro} = -\sum_{i=1}^{m} F_{hydro_i} \hat{\boldsymbol{c}}_3 \tag{34}$$

$$= -\sum_{i=1}^{m} (F_{exi} + F_{bi}) \hat{\boldsymbol{c}}_3 \tag{35}$$

$$= -\sum_{i=1}^{m} (f_{exi} \cos \omega t + \frac{(\rho_w V_s g)_i}{\cos(\pi - \psi_i)}) \hat{\boldsymbol{c}}_3 \tag{36}$$

where m is the number of volume partitions (disks), and the $-ve$ sign in the above mentioned equations arises because the hydrodynamic forces always act in the negative $\hat{\boldsymbol{c}}_3$ direction. The generalized force can be calculated using Eq. (37) [14]:

$$Q_j^{hydro} = \vec{\boldsymbol{f}}^{hydro} \cdot \frac{\delta \vec{\boldsymbol{r}}_{dma}}{\delta x_j}, \ \forall j = 1, \cdots 3+N \tag{37}$$

After substituting Eq. (36) into Eq. (37), we get:

$$\boldsymbol{Q}^{hydro} = -\sum_{i=1}^{m} \begin{bmatrix} \mathbf{0}_{2\times 1} \\ \vec{\boldsymbol{f}}_{hydro_i} \cdot \mathbf{1}_3 \\ \vec{\boldsymbol{f}}_{hydro_i} \cdot \boldsymbol{\Phi}_e(:,1) \\ \vdots \\ \vec{\boldsymbol{f}}_{hydro_i} \cdot \boldsymbol{\Phi}_e(:,N) \end{bmatrix} \tag{38}$$

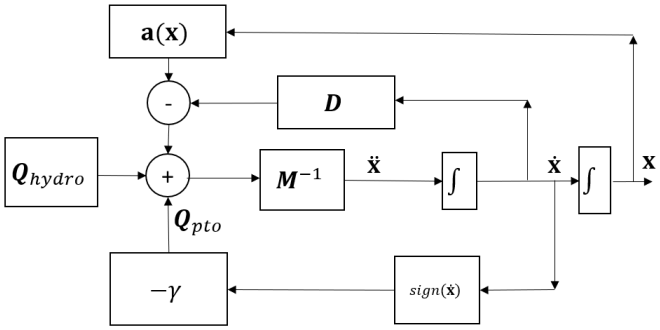

Fig. 2: Model Block Diagram

V. Results and Discussion

The radius of the WEC is 2 m, and thickness is 0.01 m. The material density, Poisson's ratio, and young's modulus of elasticity are 2700 kg/m^3, 0.3 and $2e6$ Pa, respectively. The maximum thrust used is $\gamma = 8000$, the simulation time is 60 sec, and seven truncated trial functions are used, i.e., N = 7. Fig. 2 shows a block diagram for the solution procedure and the bang bang control force calculation, where the variable time step fourth-order Runge Kutta Method is applied for the integration.

The excitation pressure around the WECs is assumed to have uniform distribution, with a periodic time of 2.5 sec. The deformation of the VSB occurs as a result of the summation of the excitation and buoyant forces. The resulted heaving velocity is shown in Fig. (3); the pk-pk velocity for the VSB is 1.09 m/sec compared to 0.96 m/sec for the FSB, i.e. an increase of 13.48 %. Also, the steady state response of the FSB and VSB WECs are in phase.

The square waves generated by bang-bang PTO control is shown Fig. (4). The control force varies from 8000 to -8000 N depending on the heave velocity sign, as explained in Eq . (27).

Figures (5) and (6) show the excitation forces in the $\hat{\boldsymbol{a}}_1$ direction and the total buoys' volume change with time. Although a similar pressure field wave is applied on both VSB and FSB, the resulting excitation force in the heave direction for the VSB decreased; however, the total WEC volume increased. From Eq. (36) both excitation and buoyant forces contribute to the buoy's total hydrodynamic forces.

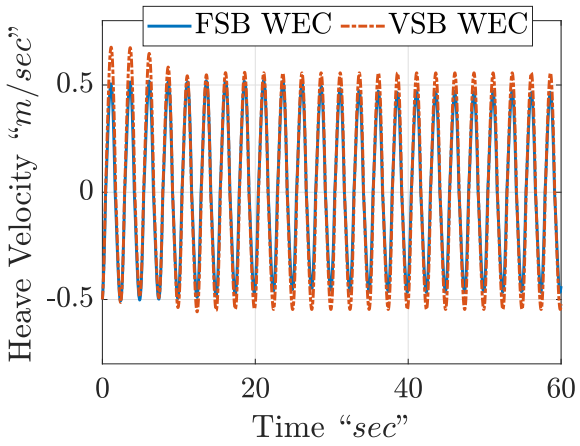

Fig. 3: Heave Velocities

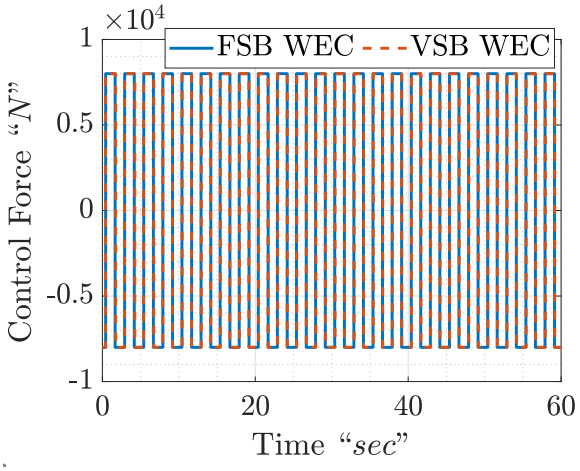

Fig. 4: PTO Force

The transient effects on the volume change are seen clearly in the first 10 seconds in Fig (6). Also, it can be noticed that after the transient effect vanishes (10 seconds), the particular solution follows the same frequency as the excitation force. The harvested energy increased 16.99% for the VSB compared to FSB.

VI. CONCLUSION

This paper derives the equation of motion for a heaving VSB WECs; the VSB shell is assumed to vibrate axi-symmetrically. The effect of bang-bang control on the performance of VSB WEC is investigated. The dynamic model was developed using the approximated modes method, and performance assessment was conducted in the vicinity of Bang Bang control system, the maximum thrust used was 8000 N, over a period of 30 seconds. Within the limitations of the assumptions made in developing the dynamic model, the results show an increase of 16.99% for harvested energy of the VSB WEC compared to the FSB WEC.

Further investigation on the performance of the VSB WEC by coupling the developed equation of motion with a fluid solver is required, the fluid solver can be either a computa-

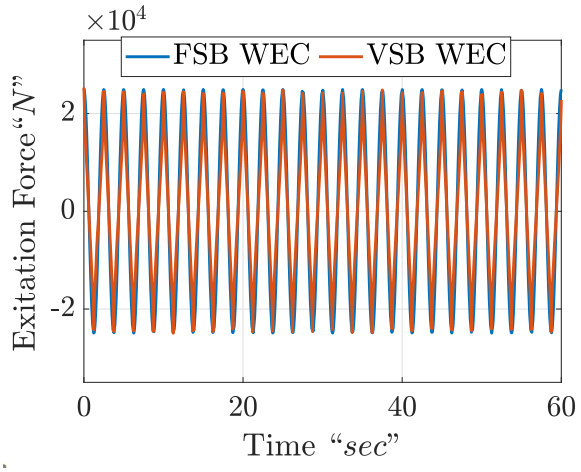

Fig. 5: Excitation Forces

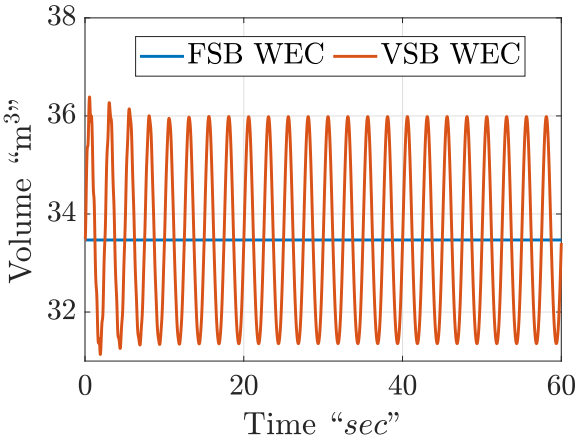

Fig. 6: Total Volume of Buoy

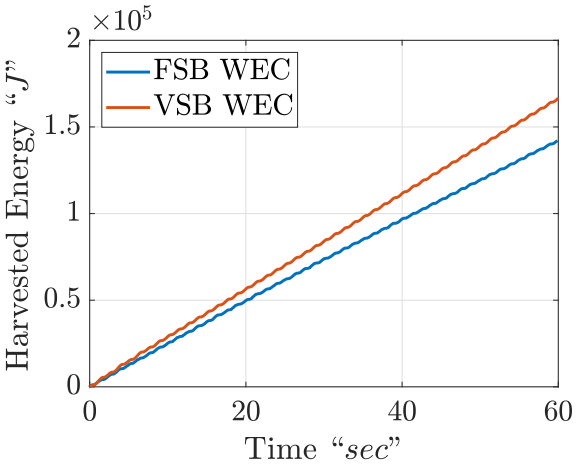

Fig. 7: Harvested Energy

tional fluid dynamics solver or a hydrodynamics solver where the added mass and radiation forces are included.

ACKNOWLEDGMENT

This material is based upon work supported by the National Science Foundation (NSF), USA, under Grant Number 2023436.

REFERENCES

[1] V. S. Arutyunov and G. V. Lisichkin, "Energy resources of the 21st century: problems and forecasts. can renewable energy sources replace fossil fuels?" *Russian Chemical Reviews*, vol. 86, no. 8, p. 777, 2017.

[2] A. Clément, P. McCullen, A. Falcão, A. Fiorentino, F. Gardner, K. Hammarlund, G. Lemonis, T. Lewis, K. Nielsen, S. Petroncini *et al.*, "Wave energy in europe: current status and perspectives," *Renewable and sustainable energy reviews*, vol. 6, no. 5, pp. 405–431, 2002.

[3] K. Mall and E. Taheri, "Optimal control of wave energy converters using epsilon-trig regularization method," in *2020 American Control Conference (ACC)*. IEEE, 2020, pp. 1773–1778.

[4] M. Shabara, S. Zou, and O. Abdelkhalik, "Numerical investigation of a variable-shape buoy wave energy converter," in *The 40th International Conference on Ocean, Offshore and Arctic Engineering, OMAE2021*, 2021. [Online]. Available: https://asmedigitalcollection.asme.org/OMAE/proceedings/OMAE2021/85192/V009T09A013/1121598

[5] J. N. Newman, "Wave effects on deformable bodies," *Applied ocean research*, vol. 16, no. 1, pp. 47–59, 1994.

[6] A. Mcdonald, Q. Xiao, D. Forehand, and R. Costello, "Linear analysis of fluid-filled membrane structures using generalised modes," in *In Proceedings of the 13th European Wave and Tidal Energy Conference, Naples, Italy*, September 2019.

[7] Y. Guo, Y.-H. Yu, J. A. van Rij, and N. M. Tom, "Inclusion of structural flexibility in design load analysis for wave energy converters," National Renewable Energy Lab.(NREL), Golden, CO (United States), Tech. Rep., 2017.

[8] E. Abraham, "Optimal control and robust estimation for ocean wave energy converters," Ph.D. dissertation, Imperial College London, 2013.

[9] S. Zou, O. Abdelkhalik, R. Robinett, G. Bacelli, and D. Wilson, "Optimal control of wave energy converters," *Renewable energy*, vol. 103, pp. 217–225, 2017.

[10] W. Soedel, *Vibrations of shells and plates*. Marcel Dekker Incorporated, 1981, vol. 10.

[11] F. R. Hogan, J. R. Forbes, and A. Walsh, "Dynamic modeling of a rolling flexible sphere," in *International Design Engineering Technical Conferences and Computers and Information in Engineering Conference*, vol. 57181. American Society of Mechanical Engineers, 2015, p. V008T13A086.

[12] S. S. Rao, *Vibration of continuous systems*. John Wiley & Sons, 2019.

[13] M. A. Shabara and O. Abdelkhalik, "Dynamic modeling of spherical variable-shape wave energy converters," 2022. [Online]. Available: https://arxiv.org/pdf/2201.08942.pdf

[14] H. Schaub and J. L. Junkins, *Analytical mechanics of space systems*. Aiaa, 2003.